Supplementary Information for

Strong plasmon-exciton coupling between lithographically defined single metal nanoparticles and monolayer WSe_2

Xiaohong Yan,[a,b] Hong Wei*[a,c]

[a]Beijing National Laboratory for Condensed Matter Physics, Institute of Physics, Chinese Academy of Sciences, Beijing 100190, China

[b]School of Physical Sciences, University of Chinese Academy of Sciences, Beijing 100049, China

[c]Songshan Lake Materials Laboratory, Dongguan 523808, China

*E-mail: weihong@iphy.ac.cn

1. WSe_2 monolayer transfer

The WSe_2 monolayers on sapphire substrate (10×10 mm) were purchased from 6Carbon Technology (Shenzhen). PMMA (950K A5) resist was spin-coated on top of the WSe_2 sample at a speed of 2000 rpm for 60 s. Then the PMMA layer was scribed to several pieces by a scalpel for leading the NaOH solution in the next step and saving the WSe_2 sample. Next, the sample was immersed in the NaOH solution (2 mol/L, 90 °C) for 30 min to etch the sapphire substrate surface contacting the WSe_2 monolayers. Then we separated the PMMA layer with the attached WSe_2 from the sapphire substrate in water and fished up each of the PMMA pieces to a clean SiO_2/Si substrate.[1] An adhesive tape with a hole which is a little smaller than the PMMA piece was used to tape up the PMMA piece. Then, the adhesive tape with the PMMA piece was carefully transferred by our home-made transfer station to the top of the gold nanostructures. The obtained sample was placed on a hot plate (130 °C) for 30 min to ensure that the WSe_2 monolayers were closely adsorbed to the substrate. Then the PMMA layer was removed by acetone. Finally,

the sample was washed by alcohol and deionized water, and dried by high purity nitrogen blow.

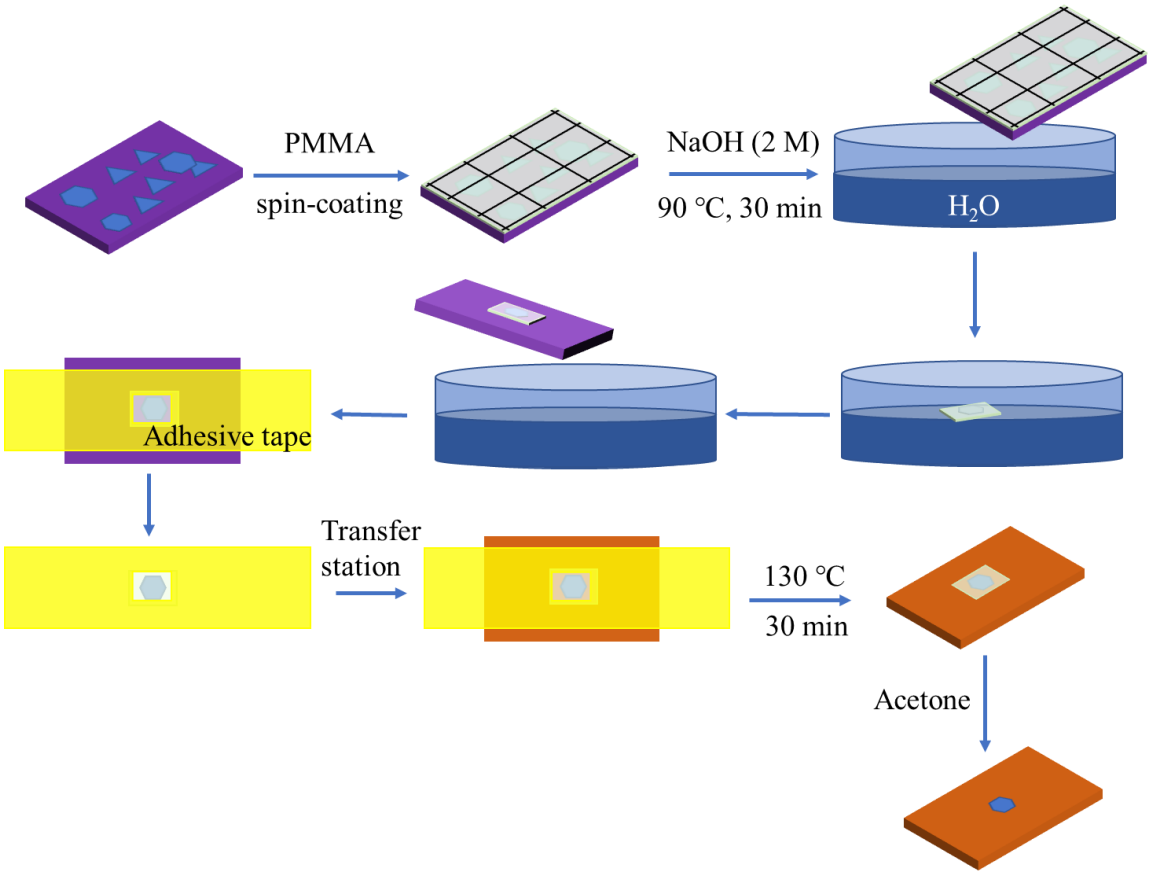

Figure S1. The schematic flow diagram of the WSe_2 monolayer transfer.

2. Bright-field optical image of gold nanobowties covered by WSe_2

We confirm the uniformity of the transferred WSe_2 by the optical contrast in the bright-field optical image, as partly shown in the top inset in Figure 1b. Figure S2 shows the complete bright-field optical image containing the area in the inset of Figure 1b.

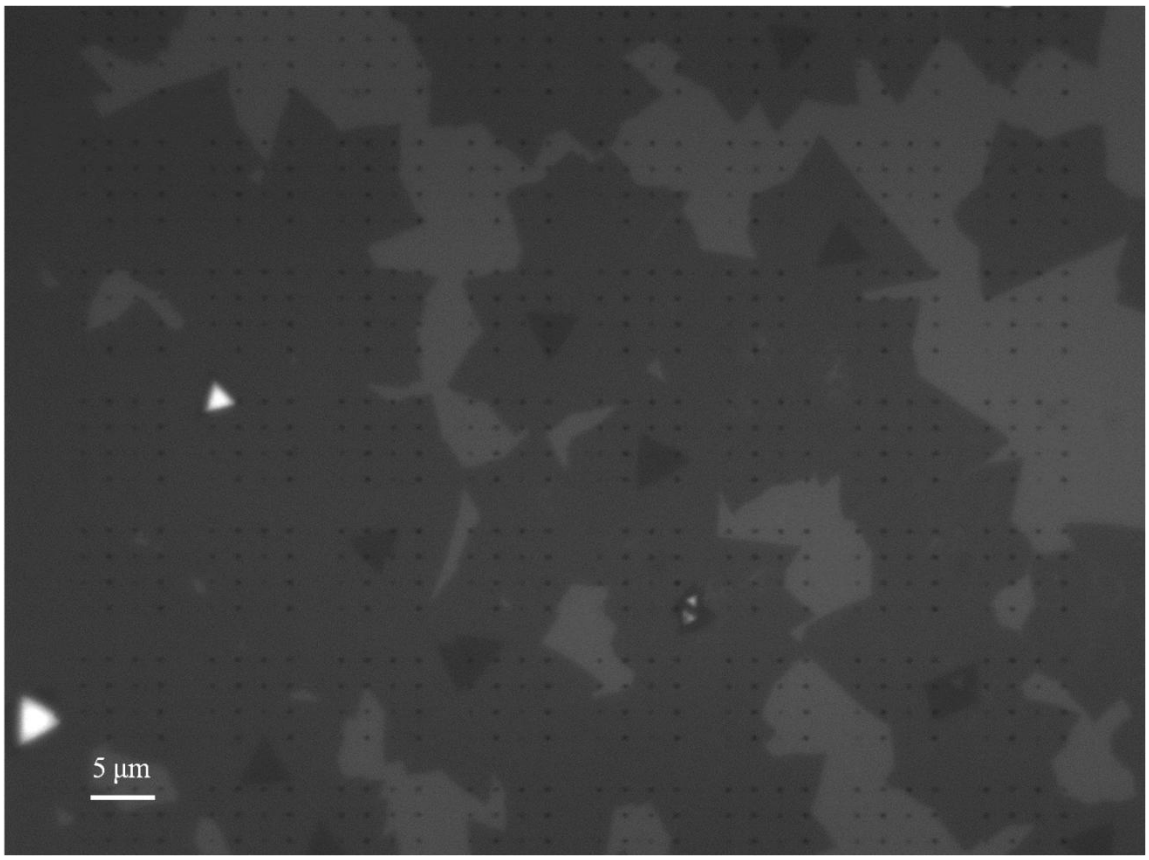

Figure S2. Bright-field optical image of gold nanobowties covered by WSe_2. The arrayed black dots indicate the gold nanobowties, the large light black areas indicate the monolayer WSe_2, and the dark black or bright triangles are the multilayer WSe_2.

3. The Raman measurements of monolayer WSe_2

To confirm the monolayer nature of the WSe_2 layer, we measured the Raman spectra of the light black area in the bright-field image in Figure S2 using a Raman spectrometer system (inVia, Renishaw) with an excitation laser of 514 nm. It's clear that there is no visible peak around 308 cm^{-1}, proving the monolayer nature of the film.[2]

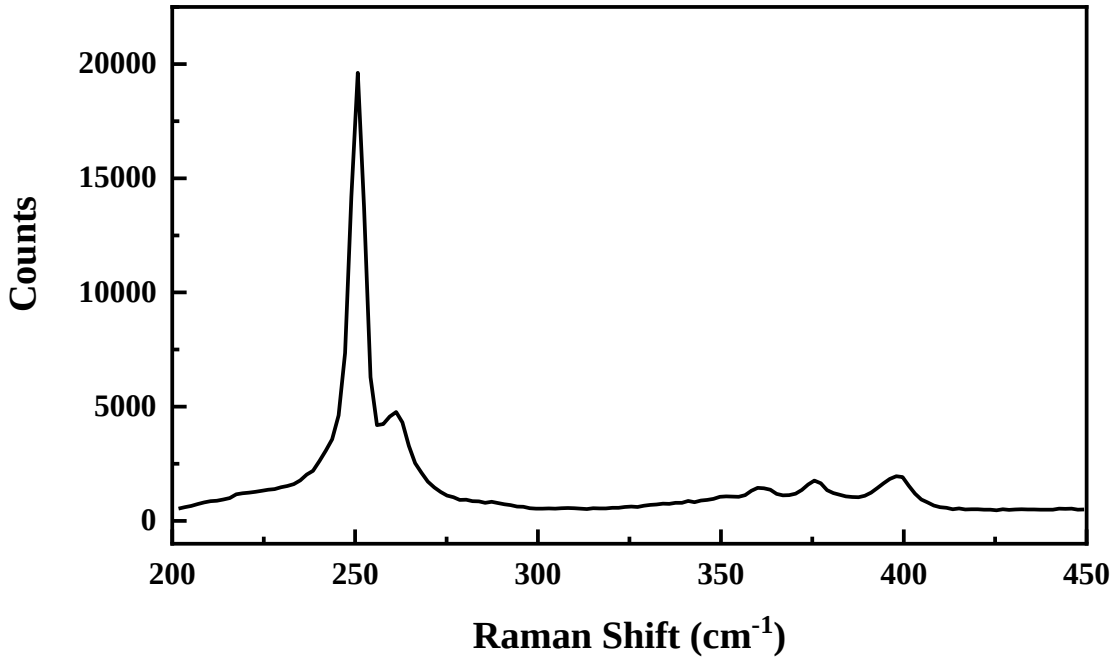

Figure S3. The Raman spectrum of the WSe_2 monolayer excited by a 514 nm laser. The laser power is 208 μW, and the exposure time is 10 s.

4. In-plane dielectric function of monolayer WSe_2

To figure out the in-plane dielectric function of monolayer WSe_2, we measured the transmission spectrum of a monolayer WSe_2 flake on top of a clean glass substrate. The schematic diagrams of the transmission measurements with and without the WSe_2 monolayer are shown in Figure S4. In the experiments, we can only measure the value I_{Air} and I. The transmission coefficient of WSe_2 monolayer T is obtained by $T = I / I_0 = T_{\mathrm{Air}} I / I_{\mathrm{Air}}$, where $T_{\mathrm{Air}} = I_{\mathrm{Air}} / I_0$ is the transmission coefficient at the glass-air interface.

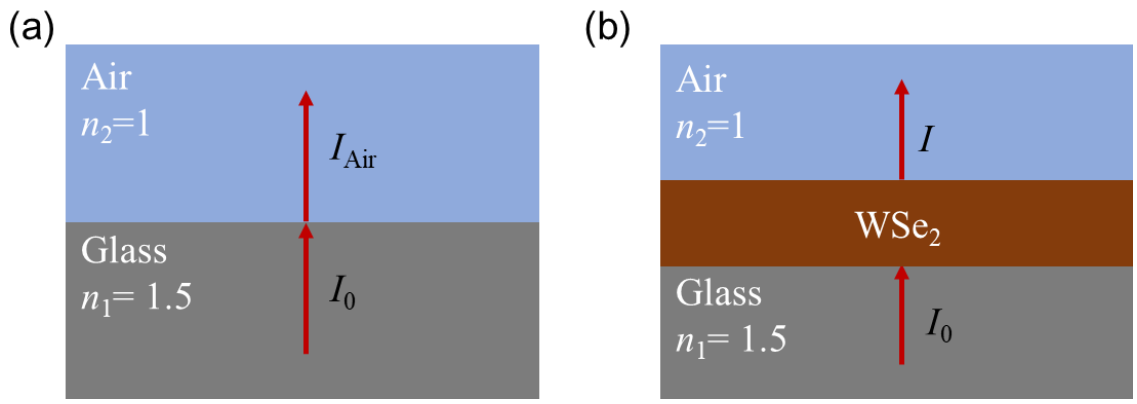

Figure S4. (a) The schematic diagram of the transmission measurement for a glass substrate. I_{Air} is the measured light intensity in the air side, and I_0 is the incident light intensity at the glass-air interface. (b) The schematic diagram of the transmission measurement for a monolayer WSe_2 flake on the glass substrate. I is the measured light intensity in the air side.

For the normal incidence, the transmission coefficient at glass-air interface can be obtained as follows:

$$T_{\text{Air}} = \frac{4n_1n_2}{(n_1+n_2)^2} = 0.96, \text{ (S1)}$$

where n_1 and n_2 are the refractive index of the glass substrate and air, respectively. Therefore, $T = I / I_0 = 0.96 I / I_{\text{Air}}$.

The transmission coefficient can be related with the refractive index of the monolayer WSe_2 $\tilde{n} = n + i\kappa$ as follows:[3]

$$T = \frac{16n_1n_2(n^2+\kappa^2)\alpha}{A + B\alpha^2 + 2\alpha[C\cos(4\pi nt/\lambda) + D\sin(4\pi nt/\lambda)]}, \text{ (S2)}$$

with

$$
\begin{aligned}
A &= [(n+n_1)^2+\kappa^2][(n+n_2)^2+\kappa^2], \\
B &= [(n-n_1)^2+\kappa^2][(n-n_2)^2+\kappa^2], \\
C &= -(n^2-{n_1}^2+\kappa^2)(n^2-{n_2}^2+\kappa^2)+4\kappa^2 n_1 n_2, \quad \text{(S3)} \\
D &= 2\kappa n_2(n^2-{n_1}^2-\kappa^2)+2\kappa n_1(n^2-{n_2}^2-\kappa^2), \\
\alpha &= \exp(-4\pi\kappa t/\lambda),
\end{aligned}
$$

where t is the thickness of the monolayer WSe_2 (0.7 nm), and λ is the wavelength of the transmitted light. The exciton states of monolayer WSe_2 are indicated in the measured transmission spectrum (scatter dots in Figure S5). Since C exciton is far from the wavelength range of our interest and B exciton is also beyond this range, to have as few variable parameters as possible, we make use of the Lorentz model with two oscillators to mimic the undefined in-plane dielectric function of monolayer WSe_2:

$$
\varepsilon_{\text{in}} = \varepsilon_\infty + f_{\text{A}} \frac{{\omega_{\text{A}}}^2}{{\omega_{\text{A}}}^2-\omega^2-i\gamma_{\text{A}}\omega} + f_{\text{B}} \frac{{\omega_{\text{B}}}^2}{{\omega_{\text{B}}}^2-\omega^2-i\gamma_{\text{B}}\omega}, \quad \text{(S4)}
$$

where ε_∞ is the background permittivity corresponding to higher energy transitions, ω_{A} (ω_{B}), γ_{A} (γ_{B}), and f_{A} (f_{B}) are the exciton transition frequency, linewidth, and reduced oscillator strength of A (B) exciton, respectively. With the relationship of the refractive index and the dielectric function, we can substitute eq (S4) into eq (S2) and fit the transmission spectrum (Figure S5).

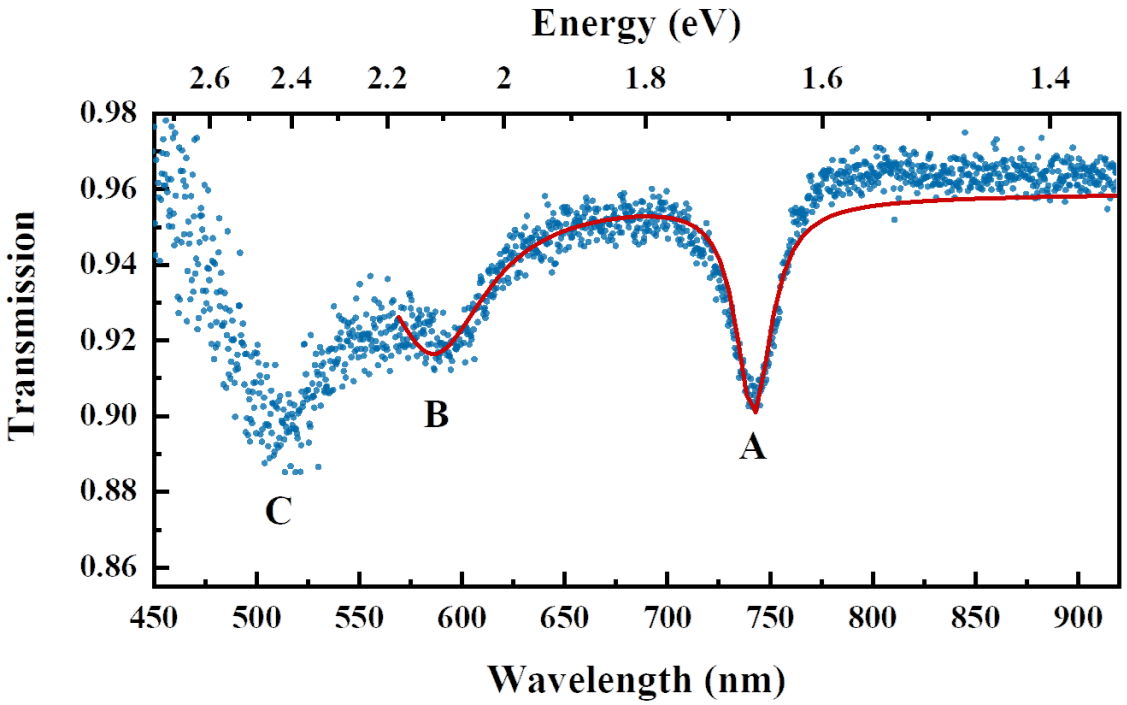

Figure S5. The transmission spectrum of the monolayer WSe_2. The scatter dots are the measured data, with the letters "A", "B", and "C" near the dips of the spectrum denoting different exciton states. The red solid line is the fitting result.

Based on the fitting results, we can plot the real and imaginary components of the in-plane dielectric function (Figure S6), which are similar with the results in literature.[4] By setting $f_A = 0$, the in-plane dielectric function in Figure S7 is obtained, which is used in the simulation for the spectral redshift of gold nanobowties induced by the dielectric layer (blue dashed lines in Figure 4a).

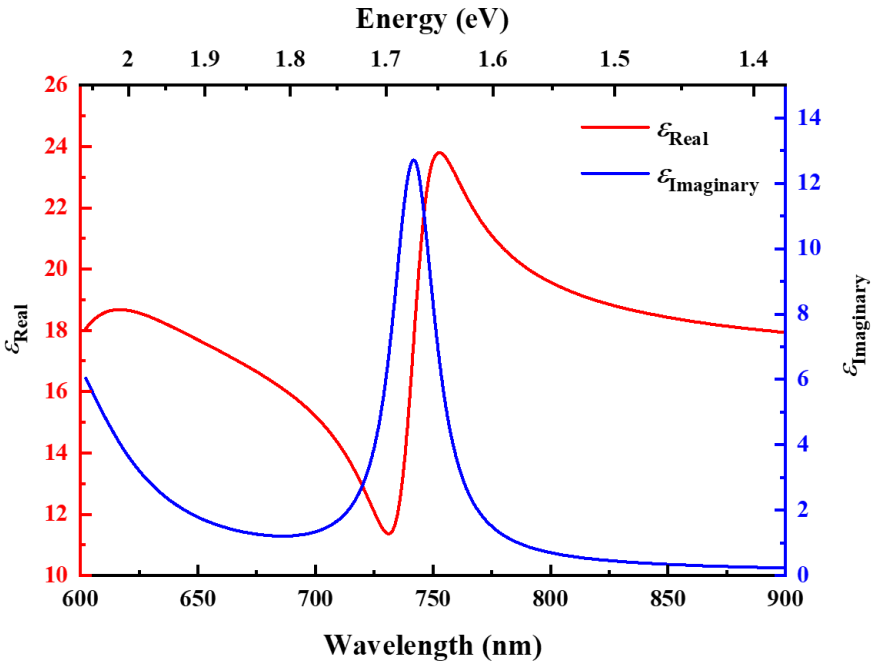

Figure S6. The real and imaginary components of the in-plane dielectric function of the monolayer WSe_2.

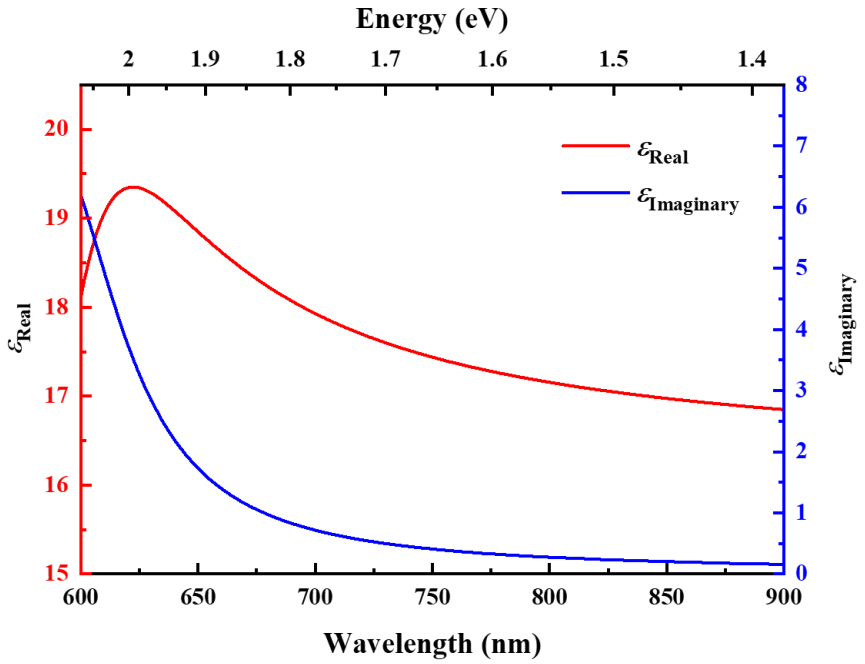

Figure S7. The real and imaginary components of the in-plane dielectric function of the monolayer WSe_2 by setting $f_A = 0$.

5. PL spectra at random positions of the transferred monolayer WSe_2 off the gold nanobowties

We measured PL spectra at several different positions in Figure S2 on the monolayer WSe_2 off the gold nanobowties, as shown in Figure S8. The peaks are all centered at about 750 nm, confirming the uniformity of exciton energy of the transferred monolayer WSe_2.

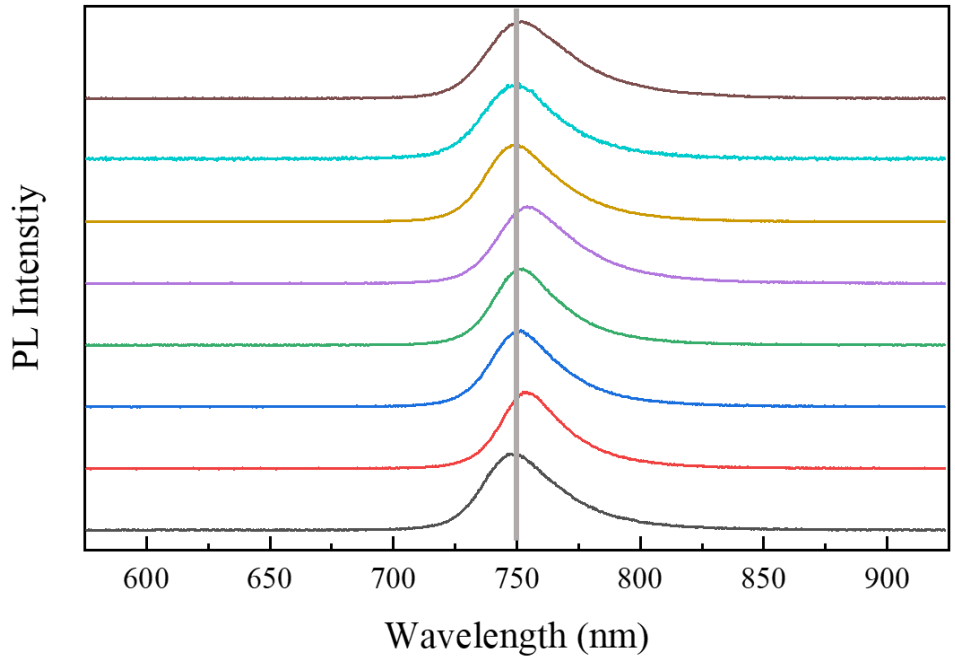

Figure S8. PL spectra at random positions of the transferred monolayer WSe_2 off the gold nanobowties. The wavelength of the excitation laser is 532 nm.

6. Coupled oscillator model

To analyze the experimental results, we adopted the coupled oscillator model:

$$\hat{H}|a\rangle = E|a\rangle . \text{ (S5)}$$

The Hamiltonian is defined as:

$$\hat{H} = \begin{pmatrix} \tilde{E}_{SP} & g \\ g & \tilde{E}_{X} \end{pmatrix}, \text{ (S6)}$$

where $\tilde{E}_{\mathrm{SP}} = E_{\mathrm{SP}} - i\frac{\Gamma_{\mathrm{SP}}}{2}$ and $\tilde{E}_{\mathrm{X}} = E_{\mathrm{X}} - i\frac{\Gamma_{\mathrm{X}}}{2}$ are the complex energies of the surface plasmon (SP) and exciton, respectively, which include the contributions of both the energy (E_{SP}, E_{X}) and linewidth (Γ_{SP}, Γ_{X}), and g is the coupling strength between the two oscillator modes.

The components of the ket-vector $|a\rangle=(a_{\mathrm{SP}}, a_{\mathrm{X}})$, i.e., a_{SP} and a_{X}, which are the complex amplitudes of each mode, are known as the Hopfield coefficients. Solving the eigenvalues of the Hamiltonian $\hat{H}$, we can get the solutions of eq (S5):

$$\tilde{E}_{\pm} = \frac{\tilde{E}_{\mathrm{SP}} + \tilde{E}_{\mathrm{X}}}{2} \pm \frac{1}{2}\sqrt{4g^2 + (\tilde{E}_{\mathrm{SP}} - \tilde{E}_{\mathrm{X}})^2} \text{ . (S7)}$$

Therefore,

$$\tilde{E}_{\mathrm{SP}} = \tilde{E}_{+} + \tilde{E}_{-} - \tilde{E}_{\mathrm{X}} \text{, (S8)}$$

$$g = \sqrt{(\tilde{E}_{+} - \tilde{E}_{\mathrm{X}})(\tilde{E}_{\mathrm{X}} - \tilde{E}_{-})} \text{, (S9)}$$

which means that we can figure out the peak energy and linewidth of the plasmon mode, as well as the coupling strength when having the peak energies and linewidths of the two plexciton states and the exciton at hand.

The detuning is defined as $\delta = E_{\mathrm{SP}} - E_{\mathrm{X}}$. In the case of zero detuning,

$$\tilde{E}_{\pm} = E_{\mathrm{X}} \pm \frac{1}{2}\sqrt{4g^2 - (\frac{\Gamma_{\mathrm{SP}} - \Gamma_{\mathrm{X}}}{2})^2} - i\frac{\Gamma_{\mathrm{SP}} + \Gamma_{\mathrm{X}}}{4} \text{, (S10)}$$

which indicates that the plexciton states are centered at $E_{\pm} = E_{\mathrm{X}} \pm \frac{1}{2}\sqrt{4g^2 - (\frac{\Gamma_{\mathrm{SP}} - \Gamma_{\mathrm{X}}}{2})^2}$, with the linewidth of $\frac{\Gamma_{\mathrm{SP}} + \Gamma_{\mathrm{X}}}{2}$.

To have a visible peak splitting, the separation between the two plexciton states, i.e., the Rabi splitting $\hbar\Omega = \sqrt{4g^2 - (\frac{\Gamma_{\mathrm{SP}} - \Gamma_{\mathrm{X}}}{2})^2}$, should exceed the linewidth of these two

branches:

$$\hbar\Omega \geq \frac{\Gamma_{SP}+\Gamma_X}{2}, \text{ (S11)}$$

which is the criterion to distinguish the strong coupling from the cavity induced transparency or Fano resonance.

When the linewidths of the uncoupled modes are much smaller than their resonance energies, we can rewrite eq (S7) as

$$E_{\pm} = \frac{E_{SP}+E_X}{2} \pm \frac{1}{2}\sqrt{4g^2+\delta^2}, \text{ (S12)}$$

which is commonly used in the literatures.[5-7] Therefore, the Rabi splitting at zero detuning can be obtained as $\hbar\Omega=2g$.

The Hopfield coefficients (a_{SP} and a_X) are obtained by solving the eigenvectors of the Hamiltonian $\hat{H}$, and the fraction of each mode is defined as the squared modulus of the corresponding Hopfield coefficient.

7. The anti-crossing behavior of monolayer WSe_2 coupling with gold nanoparticle monomers

Dark-field scattering measurements were performed for the hybrid nanostructures of monolayer WSe_2 coupling with monomers of gold nanodisks, nanotriangles, and nanorods. The peak positions of the scattering spectra of the hybrid nanostructures were extracted, and fitted by the coupled oscillator model to give the Rabi splitting energies (Figure S9). The comparison of the Rabi splitting and the mean linewidth of the SPs and excitons (Figure 3d) shows that these hybrid nanostructures are close to meeting the criterion of strong coupling.

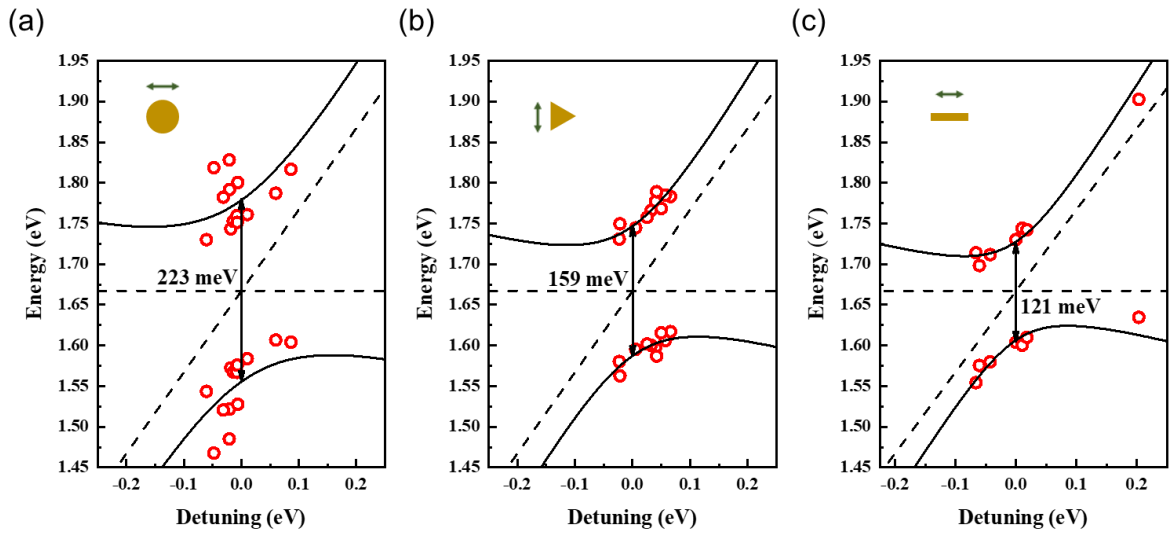

Figure S9. The peak energies of the scattering spectra as a function of detuning for the hybrid nanostructures of monolayer WSe_2 and various gold nanoparticle monomers. The fitting results (black solid lines) of the peak energies extracted from the scattering spectra (red circles) show the Rabi splitting energies of 223 meV for gold nanodisks (a), 159 meV for gold nanotriangles (b), and 121 meV for gold nanorods (c). The horizontal and tilted black dashed lines in each panel present the energies of the uncoupled exciton and plasmon mode, respectively. The green arrows denote the polarization directions relative to the gold nanostructures drawn as different golden shapes.

8. The redshift of SP resonance wavelength due to monolayer WSe_2 coating

The simulation results in Figure 4a show that the SP resonance wavelength is red-shifted by adding the dielectric layer. The red balls in Figure S10 show the redshift of the calculated spectral peaks for gold nanobowties with different SP resonance wavelengths. In experiment, the SP resonance energies of gold nanobowties coated by monolayer WSe_2 can be obtained by $E_{SP} = E_+ + E_- - E_X$, based on the scattering spectra after transferring the monolayer. The blue squares in Figure S10 show the experimental results of the redshift of the SP resonance wavelength induced by the monolayer WSe_2.

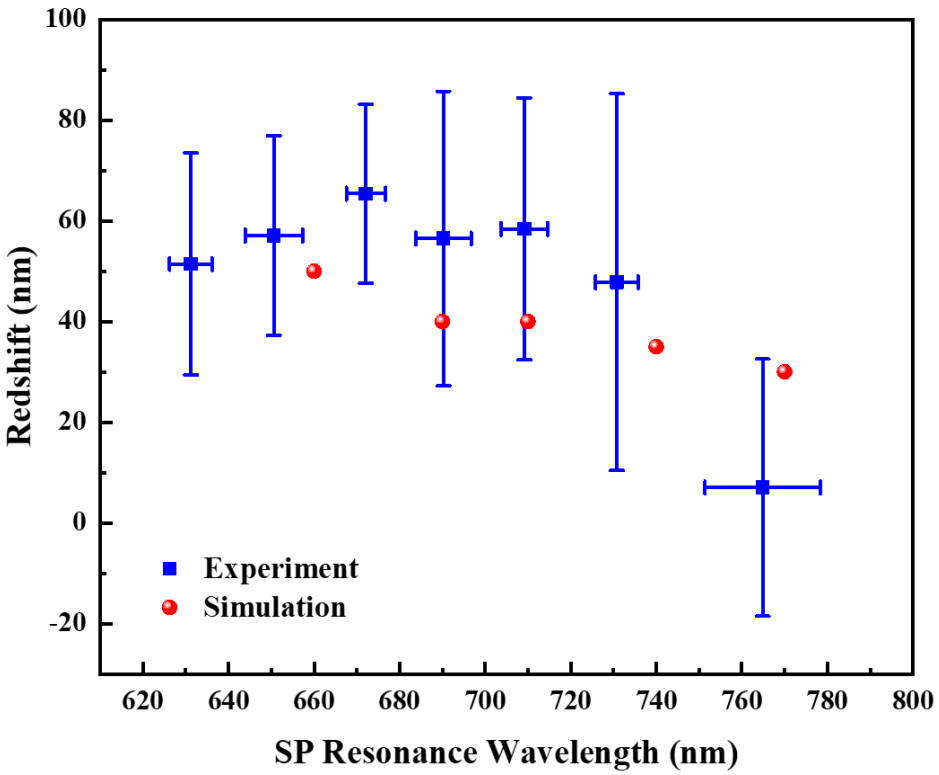

Figure S10. The redshift of SP resonance wavelength due to monolayer WSe_2 coating. The red balls are the simulation results extracted from Figure 4a. The blue squares are the mean values of experimental results for different gold nanobowties, and the error bars show the standard deviations of the experimental results.

9. Oscillator strength and transition dipole moment of monolayer WSe_2

Based on the in-plane permittivity of the monolayer WSe_2 (Figure S6), we can obtain the absorption coefficient $\alpha_{abs} = 4\pi\kappa/\lambda$, where λ is the wavelength in vacuum, and κ is the imaginary component of the refractive index and can be obtained by the permittivity. Given that the monolayer WSe_2 possesses a thickness of $t = 0.7$ nm and the exciton radius r_0 is 1 nm, we can figure out the absorption cross section of the exciton $\sigma = \alpha_{abs} / [1/(\pi r_0^2 \cdot t)]$. Thus, the frequency-integrated absorption cross section can be given by

$$\sigma_0 = \int \sigma(\omega) d\omega = 6.48857 \times 10^{12} \ (\mathrm{nm}^2/\mathrm{s}). \ (S13)$$

Then, we can get the oscillator strength f and transition dipole moment μ of the monolayer WSe_2:[8]

$$f = \frac{2\varepsilon_0 mc}{\pi e^2}\sigma_0 = 0.3891, \ (S14)$$

$$\mu = \sqrt{\frac{3}{2}\frac{g_1}{g_2}\frac{\hbar e^2}{\omega m} f} = 2.612 \times 10^{-29} \ \mathrm{Cm} = 7.835 \ \mathrm{D}, \ (S15)$$

where m and e are the mass and elementary charge of the electron, c is the speed of light, g_1 and g_2 are the degeneracy factors of the lower and upper states, respectively. The transition dipole moment of 7.835 D is similar to the result of earlier work.[7]

10. The simulated Rabi splitting and mean linewidth of uncoupled plasmon and exciton for different detuning

Figure S11 shows the simulation results for the Rabi splitting and mean linewidth of uncoupled SPs and excitons for different detuning, corresponding to nanobowties of different side lengths. Although the coupled systems with larger nanobowties possess smaller coupling strength and larger mean linewidth, the Rabi splitting is still larger than the mean linewidth, satisfying the strong coupling criterion.

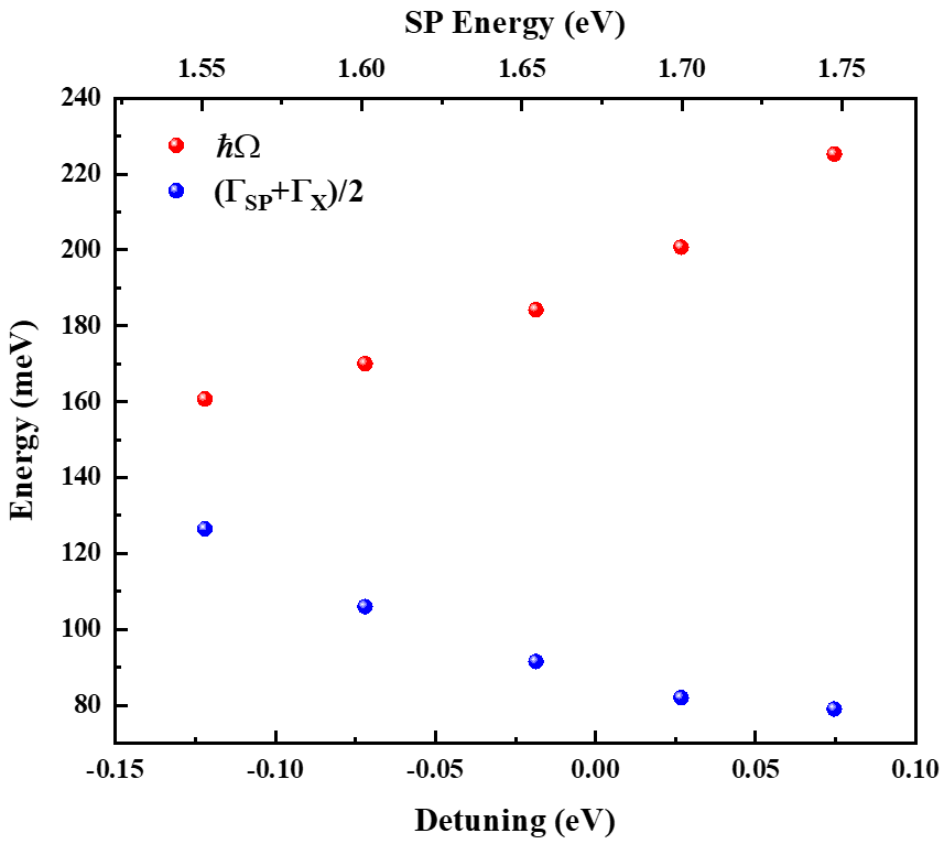

Figure S11. The simulated Rabi splitting and mean linewidth of uncoupled longitudinal SP mode of gold nanobowties and excitons of monolayer WSe_2 as a function of detuning. The side lengths of gold nanobowties are 70, 80, 90, 100, and 110 nm, respectively, from the right to left, and the gap size is kept as 10 nm.

References

1. Z. Q. Xu, Y. P. Zhang, S. H. Lin, C. X. Zheng, Y. L. Zhong, X. Xia, Z. P. Li, P. J. Sophia, M. S. Fuhrer, Y. B. Cheng and Q. L. Bao, *ACS Nano*, 2015, **9**, 6178-6187.
2. H. Li, G. Lu, Y. L. Wang, Z. Y. Yin, C. X. Cong, Q. Y. He, L. Wang, F. Ding, T. Yu and H. Zhang, *Small*, 2013, **9**, 1974-1981.
3. J. C. Manifacier, J. Gasiot and J. P. Fillard, *J. Phys. E*, 1976, **9**, 1002-1004.
4. Y. L. Li, A. Chernikov, X. Zhang, A. Rigosi, H. M. Hill, A. M. van der Zande, D. A. Chenet, E. M. Shih, J. Hone and T. F. Heinz, *Phys. Rev. B*, 2014, **90**, 205422.

5. G. Zengin, M. Wersäll, S. Nilsson, T. J. Antosiewicz, M. Käll and T. Shegai, *Phys. Rev. Lett.*, 2015, **114**, 157401.
6. R. Chikkaraddy, B. de Nijs, F. Benz, S. J. Barrow, O. A. Scherman, E. Rosta, A. Demetriadou, P. Fox, O. Hess and J. J. Baumberg, *Nature*, 2016, **535**, 127-130.
7. D. Zheng, S. P. Zhang, Q. Deng, M. Kang, P. Nordlander and H. X. Xu, *Nano Lett.*, 2017, **17**, 3809-3814.
8. R. C. Hilborn, *Am. J. Phys.*, 1982, **50**, 982-986.